

PHYSICS

Electronic structures and topological properties in nickelates $Ln_{n+1}Ni_nO_{2n+2}$

Jiacheng Gao^{1,2}, Shiyu Peng^{1,2}, Zhijun Wang ^{1,2,*}, Chen Fang^{1,3,5,*} and Hongming Weng^{1,2,3,4,*}

ABSTRACT

After the significant discovery of the hole-doped nickelate compound $Nd_{0.8}Sr_{0.2}NiO_2$, analyses of the electronic structure, orbital components, Fermi surfaces and band topology could be helpful to understand the mechanism of its superconductivity. Based on first-principle calculations, we find that Ni $3d_{x^2-y^2}$ states contribute the largest Fermi surface. The $Ln5d_{3z^2-r^2}$ states form an electron pocket at Γ , while $5d_{xy}$ states form a relatively bigger electron pocket at A. These Fermi surfaces and symmetry characteristics can be reproduced by our two-band model, which consists of two elementary band representations: $B_{1g}@1a \oplus A_{1g}@1b$. We find that there is a band inversion near A, giving rise to a pair of Dirac points along M-A below the Fermi level upon including spin-orbit coupling. Furthermore, we perform density functional theory based Gutzwiller (DFT+Gutzwiller) calculations to treat the strong correlation effect of Ni 3d orbitals. In particular, the bandwidth of $3d_{x^2-y^2}$ has been renormalized largely. After the renormalization of the correlated bands, the Ni $3d_{xy}$ states and the Dirac points become very close to the Fermi level. Thus, a hole pocket at A could be introduced by hole doping, which may be related to the observed sign change of the Hall coefficient. By introducing an additional Ni $3d_{xy}$ orbital, the hole-pocket band and the band inversion can be captured in our modified model. Besides, the nontrivial band topology in the ferromagnetic two-layer compound $La_3Ni_2O_6$ is discussed and the band inversion is associated with Ni $3d_{x^2-y^2}$ and La $5d_{xy}$ orbitals.

Keywords: nickelate superconductors, band representations, topological Dirac points, DFT+Gutzwiller calculations

INTRODUCTION

After the discovery of high- T_c superconductivity in the cuprates [1,2], mixed-valent nickelates with similar crystals and electronic configurations as cuprates have attracted a lot of attention [3]. In particular, the configuration of Ni^{+} in infinite-layer nickelates $LnNiO_2$ ($Ln = La, Nd, Pr$) is almost identical to that of Cu^{++} in the parent compounds of cuprates. Although much effort has been devoted along this direction in the past two decades, the possible superconductivity in mixed-valent nickelates remains elusive. Until very recently, the superconductivity with $T_c = 9 \sim 15$ K was discovered in hole doped $Nd_{0.8}Sr_{0.2}NiO_2$ for the first time [4]. For the parent compound $NdNiO_2$, previous studies have established several experimental facts that

are distinct from the parent compound of cuprates. First, no long-range magnetic order is observed experimentally [5,6], while an antiferromagnetically ordered state is formed in the cuprates [7]. Second, $NdNiO_2$ exhibits a metallic behavior above 50 K [4], while the parent cuprates are Mott insulators [8]. Third, the superconductivity (so far) is only found in the hole doped $Nd_{0.8}Sr_{0.2}NiO_2$, while it is found in the electron-doped cuprate $Sr_{1-x}La_xCuO_2$ in the same structure [9]. These experimental facts indicate that the ground state of the parent nickelates could have significant difference from the cuprates. Analyses of their electronic band structures, orbital components, Fermi surfaces and the band topology are needed. In addition, a minimal-band effective model is very helpful to further understand the mechanism of superconductivity.

¹Beijing National Laboratory for Condensed Matter Physics, Institute of Physics, Chinese Academy of Sciences, Beijing 100190, China; ²School of Physical Sciences, University of Chinese Academy of Sciences, Beijing 100190, China; ³Songshan Lake Materials Laboratory, Dongguan 523808, China; ⁴Physical Science Laboratory, Huairou National Comprehensive Science Center, Beijing 101407, China and ⁵Kavli Institute for Theoretical Sciences, Chinese Academy of Sciences, Beijing 100190, China

*Corresponding authors. E-mails: wzj@iphy.ac.cn; cfang@iphy.ac.cn; hmweng@iphy.ac.cn

Received 16 March 2020; Revised 26 May 2020; Accepted 27 August 2020

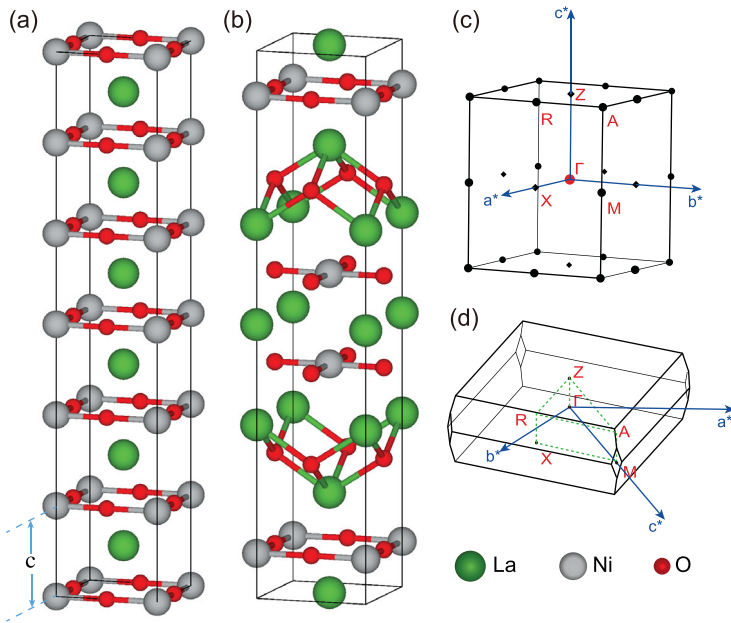


Figure 1. Crystal structures and Brillouin zones. The crystals of the two end members LaNiO_2 ($n = \infty$, $P4/mmm$) and $\text{La}_3\text{Ni}_2\text{O}_6$ ($n = 2$, $I4/mmm$) are presented in (a) and (b), respectively. The panel (a) contains six unit cells of LaNiO_2 (c is the lattice parameter in the z direction). The primitive reciprocal lattice vectors and high-symmetry k points are indicated in the first Brillouin zones of (c) LaNiO_2 and (d) $\text{La}_3\text{Ni}_2\text{O}_6$. a^* , b^* and c^* refer to the primitive reciprocal lattice vectors.

In this work, we perform detailed first-principle calculations within the framework of density functional theory (DFT). The obtained band structure of the parent (undoped) compound NdNiO_2 is similar to that of LaNiO_2 reported previously [10] and PrNiO_2 ($\text{Nd-}4f$ and $\text{Pr-}4f$ orbitals are treated as core states). In this article, LaNiO_2 is taken as a representative and the band structures of NdNiO_2 and PrNiO_2 are presented in the online supplementary material. In the undoped case, there are three bands intersecting the Fermi level (E_F), mainly from $\text{Ni } 3d_{x^2-y^2}$, $\text{La } 5d_{xy}$ and $\text{La } 5d_{3z^2-r^2}$ orbitals. They form a large cylinderlike electron pocket (EP) surrounding the Γ - Z line, a spherelike EP at A and a comparatively smaller spherelike EP at Γ , respectively. These Fermi surfaces and symmetry characteristics can be reproduced by our two-band model, which consists of two elementary band representations (EBRs): $B_{1g}@1a \oplus A_{1g}@1b$. The EBR of $B_{1g}@1a$ refers to the $3d_{x^2-y^2}$ orbital at Wyckoff site $1a[0,0,0]$, while the EBR of $A_{1g}@1b$ refers to the A_{1g} orbital at Wyckoff site $1b[0,0,0.5]$, where no atoms sit.

We find that a band inversion near A happens between the $\text{Ni } 3d_{xy}$ states and $\text{Ln } 5d_{xy}$ states (the effect of Coulomb interaction U is discussed in the online supplementary material). With small U and spin-orbital coupling (SOC), this gives rise to a pair of Dirac points along M - A . After considering

the renormalization of $\text{Ni } 3d$ bands, the Dirac point becomes very close to the charge neutrality level and accessible by hole doping. As a result, a hole pocket (HP) could emerge at A , which may be responsible for the sign change of the Hall coefficient in the experiment [4]. By introducing an additional $\text{Ni } 3d_{xy}$ orbital, the hole-pocket band and the band inversion can be captured in the modified model. Besides, the nontrivial band topology in the ferromagnetic two-layer compound $\text{La}_3\text{Ni}_2\text{O}_6$ ($n=2$) is discussed and a band inversion happens between the $\text{Ni } 3d_{x^2-y^2}$ and $\text{La } 5d_{xy}$ orbitals.

CRYSTAL STRUCTURE AND METHODOLOGY

The parent compound LaNiO_2 can be obtained from the perovskites LaNiO_3 by removing the apical oxygens (i.e. b site), as shown in Fig. 1(a). Consequently, it has a tetragonal lattice, and has the same planes as the cuprate superconductors with Ni^+ instead of Cu^{++} ions. Similarly, the two-layer nickelate $\text{La}_3\text{Ni}_2\text{O}_6$ (see Fig. 1(b)) can be produced [11] from the two-layer perovskite $\text{La}_3\text{Ni}_2\text{O}_7$. We perform first-principle calculations using the VASP package [12,13] based on density functional theory with the projector augmented wave method [14,15]. The generalized gradient approximation (GGA) and the exchange-correlation functional of Perdew, Burke and Ernzerhof [16] are employed. The kinetic energy cutoff is set to 500 eV for the plane wave basis. A $10 \times 10 \times 10$ k mesh for self-consistent Brillouin zone (BZ) sampling is adopted. The experimental lattice parameters of LaNiO_2 and $\text{La}_3\text{Ni}_2\text{O}_6$ are employed [4,11].

RESULTS AND DISCUSSIONS

Band structure and density of states

We first perform first-principle calculations on LaNiO_2 without SOC. The band structure is presented in Fig. 2(a) and the total density of states is given in Fig. 2(c). The blue dashed horizontal line corresponds to the charge neutrality level of the undoped case. The red dashed line in Fig. 2(b) is the theoretically estimated chemical potential for the 20% hole-doped superconductivity $\text{Nd}_{0.8}\text{Sr}_{0.2}\text{NiO}_2$. Moreover, the partial DOSs are also computed for $\text{O } 2p$, $\text{Ni } 3d$ and $\text{La } 5d$ orbitals, respectively. Since the main quantum numbers of different atom's orbitals are distinct, we call them $2p$, $3d$ and $5d$ orbitals (states) for short in the following discussion. From the plotted partial DOSs in Fig. 2(c), we note that $2p$ states are mainly located from -10 to -3.5 eV below E_F , while $3d$ states are around E_F , from -3.5

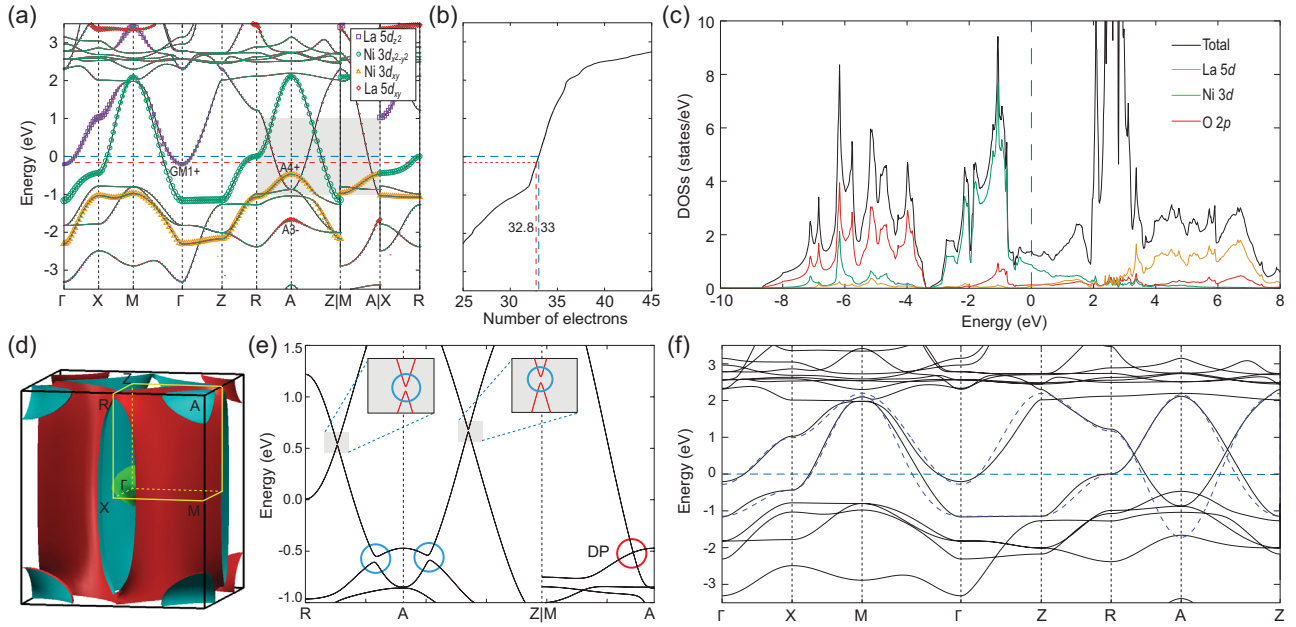


Figure 2. (a) The band structure of LaNiO_2 without SOC. The weights of the $\text{La } 5d_{z^2}$, $\text{Ni } 3d_{x^2-y^2}$, $\text{Ni } 3d_{xy}$ and $\text{La } 5d_{xy}$ states are indicated by the size of the purple squares, green circles, yellow triangles and red diamonds, respectively. The $\text{La } 5d_{z^2}$ band at Γ is labeled $\text{GM}1+$, while the $\text{Ni } 3d_{xy}$ and $\text{La } 5d_{xy}$ bands at A are labeled $\text{A}4+$ and $\text{A}3-$, respectively. The blue dashed line represents the Fermi level E_F and the red dashed line represents the estimated chemical potential in the hole-doped $\text{Nd}_{0.8}\text{Sr}_{0.2}\text{NiO}_2$. The total number of electrons as a function of the chemical potential is plotted in (b). The partial density of states (DOSs) is given in (c). The Fermi surfaces of LaNiO_2 are shown in (d). In the band structure with SOC (e), the crossings in the shadowed area of (a) are gapped except the Dirac point (DP) along M - A . The bands of our two-band model are shown as blue dashed lines in (f).

to 1.5 eV. The situation is much different from the situation in copper-based superconductors, where $\text{O } 2p$ states are slightly below E_F and hybridize strongly with $\text{Cu } 3d$ states [10]. In addition, from the orbital projections in Fig. 2(a), we note that there are $5d_{3z^2-r^2}$ states at Γ and $5d_{xy}$ states at A around E_F , suggesting that the $5d$ states are more extended, compared to the $\text{Ca } 3d$ states in CaCuO_2 [17].

Evolution of Fermi surfaces

At the charge neutrality level, we find that there are three bands crossing E_F , which are mainly from $3d_{x^2-y^2}$, $5d_{z^2}$ and $5d_{xy}$ orbitals, respectively. The weights of these orbitals are depicted by the size of the different symbols in Fig. 2(a). Therefore, as shown in Fig. 2(d), three EPs are formed: (i) the $3d_{x^2-y^2}$ orbital forms the largest electron pocket around the Γ and Z points, which has a strong two-dimensional (2D) feature; (ii) the second larger EP is nearly a sphere around A , formed by the $5d_{xy}$ orbital; (iii) the smallest EP is a sphere around Γ , formed by the $5d_{3z^2-r^2}$ orbital (which is also hybridized with the $\text{Ni } 3d_{3z^2-r^2}$ orbital in the DFT calculations, yet we still call it $5d_{3z^2-r^2}$ for simplicity).

In the hole-doped superconductor $\text{Nd}_{0.8}\text{Sr}_{0.2}\text{NiO}_2$, the estimated chemical potential of the 20% Sr-doped level is denoted by a red dashed line, which corresponds to 32.8 electrons

per unit cell (the charge neutrality level corresponds to 33 electrons). Needless to say that all the electron pockets become smaller with hole doping. In particular, the $5d_{3z^2-r^2}$ -orbital-formed Γ -centered EP is about to be removed. On the other hand, the states from the $3d_{xy}$ orbital become closer to the chemical potential, especially in the vicinity of point A .

Band inversion and Dirac points

The band crossings along R - A , A - Z and M - A are protected by m_{001} , m_{110} and C_{4z} , respectively. After considering SOC, the band crossings open small gaps (blue circles) along the mirror protected R - A and A - Z lines, but remain gapless along the C_{4z} -invariant line M - A , as shown in Fig. 2(e). The gapless Dirac points along M - A [highlighted in the red circle in Fig. 2(e)] are protected by C_{4v} symmetry. Namely, the two doubly degenerate bands belong to different 2D irreducible representations (IRs) of the C_{4v} double group. In our GGA+ U calculations, we find that the band inversion is sensitive to the value of the Coulomb interaction U , as we show in the online supplementary material.

Analysis of EBRs and orbitals

By doing an analysis of EBRs in the theory of topological quantum chemistry [18], we can also obtain

Table 1. The upper rows give the IRs for the lowest six bands in Fig. 2(a) at the maximal high-symmetry points in SG 123. The IRs are given in ascending energy order. The notation $Zm(n)$ denotes the IR m at the Z point with degeneracy n . The lower rows give the elementary band representations, labeled as $\rho@q$. Here, ρ indicates the IR supported by the orbital(s), while q stands for the Wyckoff site, where the orbital(s) is (are) located. See <https://www.cryst.ehu.es/cgi-bin/cryst/programs/bandrep.pl> [21–23] for all eBRs and IRs. The gray IRs indicate that those energy bands are at least 1.0 eV above E_F .

	A	Γ	M	Z	R	X
DFT bands	A3–(1)	GM1+(1)	M1+(1)	Z4+(1)	R4+(1)	X1+(1)
	A1+(1)	GM4+(1)	M4+(1)	Z5+(2)	R1+(1)	X4+(1)
	A5+(2)	GM5+(2)	M5+(2)		R2+(1)	X2+(1)
				Z1+(1)	R3+(1)	X3+(1)
	A4+(1)	GM2+(1)		Z2+(1)	R1+(1)	X1+(1)
	A2+(1)	GM1+(1)	M5–(2)	Z1+(1)	R2–(1)	X4–(1)
EBRs						
$A_{1g}@1a$	A1+	GM1+	M1+	Z1+	R1+	X1+
$B_{1g}@1a$	A2+	GM2+	M2+	Z2+	R1+	X1+
$B_{2g}@1a$	A4+	GM4+	M4+	Z4+	R2+	X2+
$E_g@1a$	A5+	GM5+	M5+	Z5+	R3+	X3+
					R4+	X4+
$A_{1g}@1d$	A2–	GM1+	M4+	Z3–	R3+	X4–
$B_{2g}@1d$	A3–	GM4+	M1+	Z2–	R4+	X3–
$A_{1g}@1b$	A3–	GM1+	M1+	Z3–	R2–	X1+

orbital information in real space. An EBR of $\rho@q$ is labeled by the Wyckoff position q and the IR ρ of its site symmetry group. The IRs of the six low-energy bands at maximal high symmetry k points [19,20] are computed without SOC. The results are listed in Table 1. In the crystal of LaNiO_2 , the Ni atom sits at Wyckoff position $1a[0, 0, 0]$, while the La atom sits at Wyckoff position $1d[0.5, 0.5, 0.5]$. Both Wyckoff positions have the site-symmetry group of $4/mmm$. Note that five d orbitals only support the IRs of $A_{1g}(d_{3z^2-r^2})$, $B_{1g}(d_{x^2-y^2})$, $B_{2g}(d_{xy})$ and $E_g(d_{xz}, d_{yz})$ under the single group of $4/mmm$.

The results of the EBR analysis on atomic orbitals are as follows. First, by switching the IRs of A3– and A4+ at A, we find that the four occupied bands can be represented as the sum of three EBRs: $A_{1g}@1a \oplus B_{2g}@1a \oplus E_g@1a$. Among them, the $3d_{xy}$ -based EBR $B_{2g}@1a$ has highest states at A, which may intersect with the chemical potential in the hole-doping case. Second, the band of the $3d_{x^2-y^2}$ -induced EBR $B_{1g}@1a$ is clearly shown by the weights in Fig. 2(a). There is no doubt that the $3d_{x^2-y^2}$ orbital contributes the largest Fermi surface. Third, the IR GM1+ at Γ is from the $5d_{3z^2-r^2}$ -induced EBR $A_{1g}@1d$. Last, the inverted IR A3– is from the $5d_{xy}$ -induced EBR $B_{2g}@1d$. So far, all of the orbital compounds are consistent with our DFT calculations in Fig. 2(a).

We now aim to construct a minimal effective model to reproduce the bands and symmetry characteristics near E_F . Besides the $3d_{x^2-y^2}$ -induced EBR of $B_{1g}@1a$, the two IRs of A3– and GM1+

can be generated in the EBR of $A_{1g}@1b[0,0,0.5]$. Therefore, we derive a two-band model, consisting of two EBRs: $B_{1g}@1a \oplus A_{1g}@1b$, which reproduces the exact IRs of the bands near E_F from the DFT calculations. Even through there is no actual atomic orbital at Wyckoff position $1b$ (the apical oxygens are removed), it could be formed by the hybridization of the atomic orbitals on other sites. The two-band model will be constructed for the undoped case in the following section.

Two-band effective model

Under the basis of the B_{1g} orbital at the $1a$ Wyckoff position and the A_{1g} orbital at the $1b$ Wyckoff position, the tight binding model is constructed as follows. The diagonal terms in the Hamiltonian are

$$\begin{aligned}
 T_{\alpha\alpha} = & t_{\alpha\alpha}^{(0,0,0)} + 2t_{\alpha\alpha}^{(1,0,0)}[\cos(k_x) + \cos(k_y)] \\
 & + 2t_{\alpha\alpha}^{(0,0,1)} \cos(k_z) \\
 & + 4t_{\alpha\alpha}^{(1,1,0)} \cos(k_x) \cos(k_y) \\
 & + 4t_{\alpha\alpha}^{(1,0,1)} \cos(k_z)[\cos(k_x) + \cos(k_y)] \\
 & + 8t_{\alpha\alpha}^{(1,1,1)} \cos(k_x) \cos(k_y) \cos(k_z), \quad (1)
 \end{aligned}$$

where $\alpha = 1, 2$ represent the B_{1g} orbital and the A_{1g} orbital, respectively. Here $t_{\beta\alpha}^{(l,m,n)}$ stands for the hopping parameter from orbital β of the original cell to

Box 1. The hopping parameters for the two-band and three-band model Hamiltonians.

Parameters for the two-band model							
$t_{11}^{(0,0,0)}$	0.1470	$t_{22}^{(0,0,0)}$	0.8318	$t_{21}^{(1,0,0)}$	0.0098		
$t_{11}^{(1,0,0)}$	-0.4125	$t_{22}^{(1,0,0)}$	0.0913				
$t_{11}^{(0,0,1)}$	-0.0538	$t_{22}^{(0,0,1)}$	0.0650				
$t_{11}^{(1,1,0)}$	0.0894	$t_{22}^{(1,1,0)}$	-0.0606				
$t_{11}^{(1,0,1)}$	0.0000	$t_{22}^{(1,0,1)}$	0.1988				
$t_{11}^{(1,1,1)}$	0.0134	$t_{22}^{(1,1,1)}$	0.0281				
Parameters for the three-band model							
$t_{11}^{(0,0,0)}$	0.0100	$t_{22}^{(0,0,0)}$	0.8280	$t_{33}^{(0,0,0)}$	-0.7960	$t_{21}^{(1,0,0)}$	0.0098
$t_{11}^{(1,0,0)}$	0.0042	$t_{22}^{(1,0,0)}$	-0.0510	$t_{33}^{(1,0,0)}$	-0.1655	$t_{31}^{(1,0,0)}$	-0.0132
$t_{11}^{(0,0,1)}$	0.0378	$t_{22}^{(0,0,1)}$	-0.0079	$t_{33}^{(0,0,1)}$	-0.0360	$t_{32}^{(1,1,1)}$	0.0001
$t_{11}^{(1,1,0)}$	0.0043	$t_{22}^{(1,1,0)}$	0.0105	$t_{33}^{(1,1,0)}$	-0.0497		
$t_{11}^{(1,0,1)}$	-0.1338	$t_{22}^{(1,0,1)}$	0.0000	$t_{33}^{(1,0,1)}$	0.0105		
$t_{11}^{(1,1,1)}$	0.0038	$t_{22}^{(1,1,1)}$	0.0018	$t_{33}^{(1,1,1)}$	-0.0113		

α of the (l, m, n) cell:

$$t_{\beta\alpha}^{(l,m,n)} \equiv \langle \beta; 000 | \hat{H} | \alpha; lmn \rangle. \quad (2)$$

In the off-diagonal term, the nearest and next-nearest hoppings between different orbitals are given as

$$S = t_{21}^{(1,0,0)} (1 + e^{ik_z}) [4 \cos(k_x) - 4 \cos(k_y)]. \quad (3)$$

Thus, our two-band model Hamiltonian is written as

$$H_2(k) = \begin{pmatrix} T_{11} & \dagger \\ S & T_{22} \end{pmatrix}, \quad (4)$$

where the dagger symbol means the Hermitian conjugate of the lower left part of the Hamiltonian matrix (same below). The fitting results are shown as blue dashed lines in Fig. 2(f) and the parameters can be found in Box 1. This two-band model can reproduce all the Fermi surfaces and symmetry characteristics obtained from the DFT calculations. It can be used for further study of superconductivity in the systems.

DFT+Gutzwiller method

To treat the correlation effect of five Ni 3d orbitals, we employ the DFT+Gutzwiller method [24,25]. The corresponding Gutzwiller trial wave function has been constructed as $|G\rangle = \hat{P}|0\rangle$ with

$$\hat{P} = \prod_i \hat{P}_i = \prod_i \sum_{\Gamma\Gamma'} \lambda_{i;\Gamma\Gamma'} |i, \Gamma\rangle \langle i, \Gamma'|, \quad (5)$$

where $|0\rangle$ is the noninteracting wave function and \hat{P} is the Gutzwiller local projector with $|i, \Gamma\rangle$ the atomic eigenvectors on site i . The $\lambda_{i;\Gamma\Gamma'}$ are the so-called Gutzwiller variational parameters that adjust the weights of different local atomic configurations. Ground states are obtained by minimizing the total energy $E = \langle G | (H_{tb} + H_{dc} + H_{int}) | G \rangle$ with some Gutzwiller constraints. The non-interacting Hamiltonian (H_{tb}) is extracted using the Wannier90 package [26] from the DFT calculations without SOC, which contains two La $5d_{3z^2-r^2,xy}$ orbitals and five Ni 3d orbitals. The double-counting term H_{dc} is given self-consistently. The on-site interacting term takes the Slater–Kanamori rotationally invariant atomic interaction [27]

$$\begin{aligned} H_{int} = & U \sum_{\alpha} \hat{n}_{\alpha\uparrow} \hat{n}_{\alpha\downarrow} + \frac{U'}{2} \sum_{a \neq b} \sum_{\sigma\sigma'} \hat{n}_{a\sigma} \hat{n}_{b\sigma'} \\ & - \frac{J}{2} \sum_{a \neq b} \sum_{\sigma} c_{a\sigma}^{\dagger} c_{a-\sigma} c_{b-\sigma}^{\dagger} c_{b\sigma} \\ & - \frac{J'}{2} \sum_{a \neq b} c_{a\uparrow}^{\dagger} c_{a\downarrow}^{\dagger} c_{b\uparrow} c_{b\downarrow}, \end{aligned} \quad (6)$$

where $c_{a\sigma}^{\dagger} (c_{a\sigma})$ creates (annihilates) an electron in the state of the orbital a and the spin σ , and $\hat{n}_{a\sigma} = c_{a\sigma}^{\dagger} c_{a\sigma}$.

For simplicity, we adopt diagonal variational parameters, which mean that $\lambda_{i;\Gamma\Gamma'} = \lambda_{i;\Gamma\Gamma} \delta_{\Gamma\Gamma'}$ here. Five Ni 3d orbitals are treated as correlated orbitals in the calculations (which correspond to 10 bands upon considering the spin degree of freedom). We take a Coulomb interaction U of 5 eV, Hund's coupling J of $0.18U$, where $U' = U - 2J$ and $J' = J$. Besides, the occupancy of Ni 3d orbitals has been forced to be 8.462 obtained from the DFT calculations. The results show that the quasiparticle weight

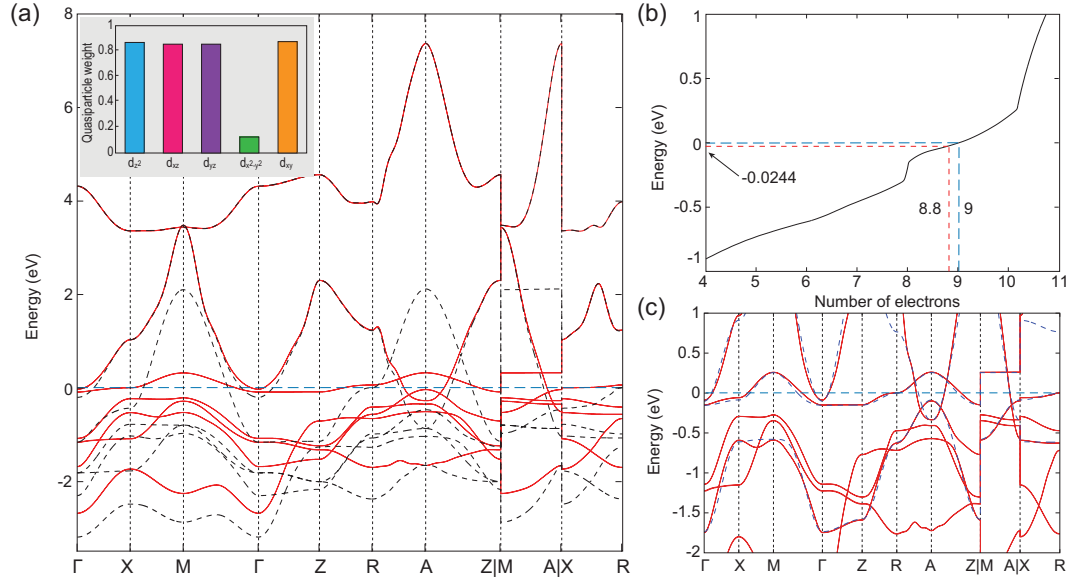


Figure 3. (a) The band structure of the noninteracting tight-binding Hamiltonian H_{tb} , extracted by the Wannier90 package, is given by black dashed lines, while the DFT+Gutzwiller bands are plotted in red solid lines. The inset of (a) shows the quasiparticle weights of five $3d$ orbitals. In panel (b) we show the total number of electrons as a function of the chemical potential in the DFT+Gutzwiller band structure. In panel (c), the bands of the three-band model are given by blue dashed lines.

of the $d_{x^2-y^2}$ orbital is very small, 0.12, while the weights of the other four orbitals are about 0.85. After considering the renormalization of the correlated $3d$ orbitals, the modified band structure is obtained and shown in Fig. 3(a). Two significant features are found after the Gutzwiller correction: (i) the bandwidth of $3d_{x^2-y^2}$ has been largely renormalized, leading to a DOS peak around E_F , which may contribute to the large peak around zero energy in the resonant inelastic X-ray scattering spectrum (RIXS) [28]; (ii) the $3d_{xy}$ states near the A point become very close to E_F . As a result, a HP could be induced by hole doping, which may be related to the observed sign change of the Hall coefficient.

In addition, the band inversion between the $3d_{xy}$ states and $5d_{xy}$ states near the A point could be important in the hole-doped nickelate compound $\text{Nd}_{0.8}\text{Sr}_{0.2}\text{NiO}_2$, since they are very close to E_F . Therefore, we modify our model by simply adding an additional $3d_{xy}$ orbital to capture the potential band inversion in this hole-doped compound. The modified model is written as

$$H_3(k) = \begin{pmatrix} T_{11} & & \dagger \\ S & T_{22} & \\ W & P & T_{33} \end{pmatrix} \quad (7)$$

with

$$P = 4t_{31}^{(1,0,0)}(1 + e^{ik_z})[\cos(k_x) - \cos(k_y)],$$

$$W = 8t_{32}^{(1,1,1)}\cos(k_x)\cos(k_y)\cos(k_z).$$

The parameters are obtained by fitting with the renormalized bands, as shown in Box 1. The results of the modified model $H_3(k)$ are shown as blue dashed lines in Fig. 3(c), which fit very well with the DFT+Gutzwiller bands, which can be compared with the angle-resolved photoemission spectroscopy (ARPES) experimental data. In any case, a four-band model constructed totally from the real atomic orbitals is presented in the online supplementary material.

Ferromagnetic state in $\text{La}_3\text{Ni}_2\text{O}_6$

To better understand the electronic structures of T' -type $\text{La}_{n+1}\text{Ni}_n\text{O}_{2n+2}$ compounds ($n \geq 2$), we calculate the other end member $\text{La}_3\text{Ni}_2\text{O}_6$ (i.e. $n = 2$ corresponds to the most reduced case) [29,30]. The ferromagnetic band structure of $\text{La}_3\text{Ni}_2\text{O}_6$ with SOC is shown in Fig. 4(a). The z -oriented magnetism [31] reduces the symmetry from type-II magnetic SG 139 to type-I magnetic SG 87. Near the M/A point, the four downward parabolic bands (i.e. 89–92 bands) are mainly from the $3d_{x^2-y^2}$ states of Ni atoms in two planar Ni–O layers, while the two upward parabolic bands (i.e. 93–94 bands) are mainly from the $5d_{xy}$ states of the La atoms sandwiched by two Ni–O planes (Fig. 1(b)). Looking closely at the crossings between the 90th and 91st bands in Fig. 4(b), we find that there is a gap along X–M (R–A), while there are two crossing points along M– Γ (A–Z). These crossing points are

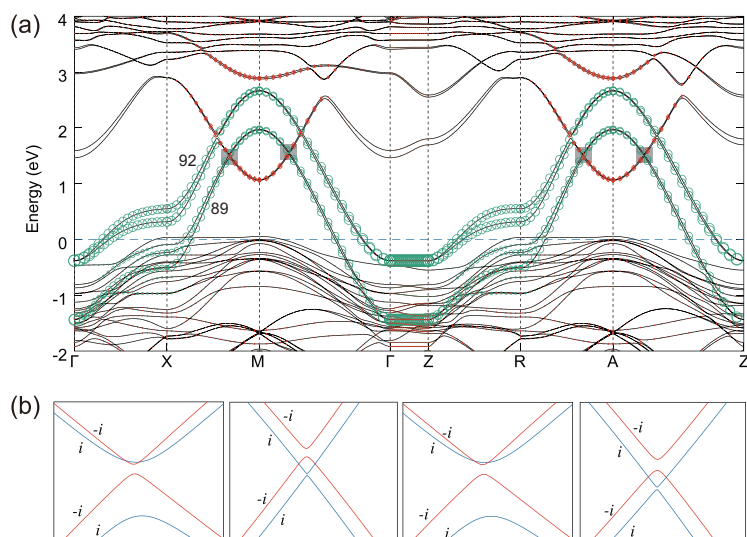


Figure 4. (a) The ferromagnetic band structure of the $\text{La}_3\text{Ni}_2\text{O}_6$ with SOC. The weights of $\text{La } 5d_{xy}$ and $\text{Ni } 3d_{x^2-y^2}$ states are indicated by the size of red diamonds and green circles, respectively. (b) The crossing points between 90th and 91st bands. Bands with different mirror eigenvalues are shown as blue (for $+i$) and red (for $-i$) lines.

parts of the tiny M_z -protected nodal rings at the $k_z = 0, 2\pi/c$ planes, which can be easily removed by very small perturbations (without changing the ordering of energy bands at high symmetry k points). According to symmetry indicators defined in magnetic systems [32], insulators in type-I MSG 87 are characterized by the indicators $\mathbb{Z}_4 \times \mathbb{Z}_4$ [33,34], which can be explained by two mirror Chern numbers in the $k_z = 0$ plane. By using the C_4 eigenvalues [35], we find that the Chern numbers are 0 and 2 for the mirror eigenvalue $+i$ and $-i$ sectors, respectively, which indicate that nontrivial edge states can emerge on the M_z -preserving surfaces.

CONCLUSION

Based on our first-principle calculations, we find that in the undoped case there are three EPs: the largest EP coming from the $\text{Ni } 3d_{x^2-y^2}$ orbital, a small EP at Γ from the $\text{La } 5d_{3z^2-r^2}$ orbital and a relatively larger EP at A from $\text{La } 5d_{xy}$. These Fermi surfaces and symmetry characteristics can be reproduced by our two-band model, which consists of two elementary band representations: $B_{1g}@1a \oplus A_{1g}@1b$. This two-band model could be used for further study of superconductivity in these systems. In the obtained band structure, a band inversion occurred at A, which gives rise to a pair of Dirac points along M-A upon including SOC. The correlation effect of $\text{Ni } 3d$ orbitals has been estimated in our DFT+Gutzwiller calculation, and the renormalized band structure obtained, which shows that $\text{Ni } 3d_{xy}$ states become very close to E_F around A. A hole pocket is likely induced by hole

doping, which may be related to the observed sign change of the Hall coefficient. The potential hole pocket and the band inversion can be captured in the modified model by simply including another $\text{Ni } 3d_{xy}$ orbital. In addition, we show that the nontrivial band topology in the ferromagnetic two-layer compound $\text{La}_3\text{Ni}_2\text{O}_6$ is associated with $\text{Ni } 3d_{x^2-y^2}$ and $\text{La } 5d_{xy}$ orbitals.

Note added. While finalizing the present paper, similar works on nickelates were published [36–40].

SUPPLEMENTARY DATA

Supplementary data are available at [NSR](#) online.

ACKNOWLEDGEMENTS

We thank Jinguang Cheng for drawing our attention to this subject and valuable discussions, as well as critical reading of this work.

FUNDING

This work was supported by the National Natural Science Foundation of China (11974395, 11504117, 11774399, 11622435, U1832202, 11921004, 11925408 and 11674370), the Beijing Natural Science Foundation (Z180008), the Ministry of Science and Technology of China (2016YFA0300600, 2016YFA0401000, 2018YFA0305700 and 2016YFA0302400), the Strategic Priority Research Program of Chinese Academy of Sciences (XXH13506-202 and XDB33000000), the Beijing Municipal Science and Technology Commission (Z181100004218001, Z171100002017018) and the Center for Materials Genome. H.W. acknowledges support from the K. C. Wong Education Foundation (GJTD-2018-01). Z.W. acknowledges support from the CAS Pioneer Hundred Talents Program and the National Thousand-Young-Talents Program.

AUTHOR CONTRIBUTIONS

H.W., C.F. and Z.W. proposed and supervised the project. J.G. carried out the DFT calculations and built the effective models. J.G. and Z.W. did the symmetry analysis. S.P. performed the DFT+Gutzwiller calculations. All authors contributed to analyzing the results and writing the manuscript.

Conflict of interest statement. None declared.

REFERENCES

1. Bednorz JG and Müller KA. Possible high T_c superconductivity in the Ba-La-Cu-O system. *Eur Phys J B* 1986; **64**: 189–93.
2. Wu MK, Ashburn JR and Torng CJ *et al.* Superconductivity at 93 K in a new mixed-phase Y-Ba-Cu-O compound system at ambient pressure. *Phys Rev Lett* 1987; **58**: 908–10.
3. Anisimov VI, Bukhvalov D and Rice TM. Electronic structure of possible nickelate analogs to the cuprates. *Phys Rev B* 1999; **59**: 7901–6.

4. Li D, Lee K and Wang BY *et al.* Superconductivity in an infinite-layer nickelate. *Nature* 2019; **572**: 624–7.
5. Hayward M, Green M and Rosseinsky M *et al.* Sodium hydride as a powerful reducing agent for topotactic oxide deintercalation: synthesis and characterization of the nickel (II) oxide LaNiO_2 . *J Am Chem Soc* 1999; **121**: 8843–54.
6. Hayward M and Rosseinsky M. Synthesis of the infinite layer Ni (II) phase NdNiO_{2+x} by low temperature reduction of NdNiO_3 with sodium hydride. *Solid State Sci* 2003; **5**: 839–50.
7. Motoyama E, Yu G and Vishik I *et al.* Spin correlations in the electron-doped high-transition-temperature superconductor $\text{Nd}_{2-x}\text{Ce}_x\text{CuO}_{4\pm\delta}$. *Nature* 2007; **445**: 186–9.
8. Lee PA, Nagaosa N and Wen XG. Doping a Mott insulator: physics of high-temperature superconductivity. *Rev Mod Phys* 2006; **78**: 17–85.
9. Smith M, Manthiram A and Zhou J *et al.* Electron-doped superconductivity at 40 K in the infinite-layer compound $\text{Sr}_{1-y}\text{Nd}_y\text{CuO}_2$. *Nature* 1991; **351**: 549–51.
10. Lee KW and Pickett W. Infinite-layer LaNiO_2 : Ni^{1+} is not Cu^{2+} . *Phys Rev B* 2004; **70**: 165109.
11. Poltavets VV, Greenblatt M and Fecher GH *et al.* Electronic properties, band structure, and Fermi surface instabilities of $\text{Ni}^{1+}/\text{Ni}^{2+}$ nickelate $\text{La}_3\text{Ni}_2\text{O}_6$, isoelectronic with superconducting cuprates. *Phys Rev Lett* 2009; **102**: 046405.
12. Kresse G and Furthmüller J. Efficiency of ab-initio total energy calculations for metals and semiconductors using a plane-wave basis set. *Comput Mater Sci* 1996; **6**: 15–50.
13. Kresse G and Furthmüller J. Efficient iterative schemes for ab initio total-energy calculations using a plane-wave basis set. *Phys Rev B* 1996; **54**: 11169–86.
14. Blöchl PE. Projector augmented-wave method. *Phys Rev B* 1994; **50**: 17953–79.
15. Kresse G and Joubert D. From ultrasoft pseudopotentials to the projector augmented-wave method. *Phys Rev B* 1999; **59**: 1758–75.
16. Perdew JP, Burke K and Ernzerhof M. Generalized gradient approximation made simple. *Phys Rev Lett* 1996; **77**: 3865–8.
17. Wu H, Zheng Q-Q and Gong X-G *et al.* The electronic structure of CaCuO_2 and SrCuO_2 . *J Phys Condens Matter* 1999; **11**: 4637–46.
18. Bradlyn B, Elcoro L and Cano J *et al.* Topological quantum chemistry. *Nature* 2017; **547**: 298–305.
19. Gao J, Wu Q and Persson C *et al.* Irvsp: to obtain irreducible representations of electronic states in the VASP. arXiv:2002.04032.
20. Vergniory M, Elcoro L and Felser C *et al.* A complete catalogue of high-quality topological materials. *Nature* 2019; **566**: 480–5.
21. Aroyo MI, Perez-Mato JM and Orobengoa D *et al.* Crystallography online: Bilbao crystallographic server. *Bulg Chem Commun* 2011; **43**: 183–97.
22. Aroyo MI, Perez-Mato JM and Capillas C *et al.* Bilbao crystallographic server: I. Databases and crystallographic computing programs. *Zeitschrift für Kristallographie* 2006; **221**: 15–27.
23. Aroyo MI, Kirov A and Capillas C *et al.* Bilbao crystallographic server. II. Representations of crystallographic point groups and space groups. *Acta Crystallogr A* 2006; **62**: 115–28.
24. Deng X, Wang L and Dai X *et al.* Local density approximation combined with Gutzwiller method for correlated electron systems: formalism and applications. *Phys Rev B* 2009; **79**: 075114.
25. Du L, Huang L and Dai X. Metal-insulator transition in three-band Hubbard model with strong spin-orbit interaction. *Eur Phys J B* 2013; **86**: 94.
26. Marzari N, Mostofi AA and Yates JR *et al.* Maximally localized Wannier functions: theory and applications. *Rev Mod Phys* 2012; **84**: 1419–75.
27. Lanatà N, Strand HUR and Dai X *et al.* Efficient implementation of the Gutzwiller variational method. *Phys Rev B* 2012; **85**: 035133.
28. Hepting M, Li D and Jia C *et al.* Electronic structure of the parent compound of superconducting infinite-layer nickelates. *Nat Mater* 2020; **19**: 381–5.
29. Manthiram A, Tang J and Manivannan V. Factors influencing the stabilization of Ni^{1+} in perovskite-related oxides. *J Solid State Chem* 1999; **148**: 499–507.
30. Poltavets VV, Lokshin KA and Dikmen S *et al.* $\text{La}_3\text{Ni}_2\text{O}_6$: a new double T'-type nickelate with infinite $\text{Ni}^{1+/2+}\text{O}_2$ layers. *J Am Chem Soc* 2006; **128**: 9050–1.
31. Sarkar S, Dasgupta I and Greenblatt M *et al.* Electronic and magnetic structures of bilayer $\text{La}_3\text{Ni}_2\text{O}_6$ and trilayer $\text{La}_4\text{Ni}_3\text{O}_8$ nickelates from first principles. *Phys Rev B* 2011; **84**: 180411.
32. Turner AM, Zhang Y and Mong RSK *et al.* Quantized response and topology of magnetic insulators with inversion symmetry. *Phys Rev B* 2012; **85**: 165120.
33. Po HC, Vishwanath A and Watanabe H. Symmetry-based indicators of band topology in the 230 space groups. *Nat Commun* 2017; **8**: 50.
34. Ono S and Watanabe H. Unified understanding of symmetry indicators for all internal symmetry classes. *Phys Rev B* 2018; **98**: 115150.
35. Fang C, Gilbert MJ and Bernevig BA. Bulk topological invariants in noninteracting point group symmetric insulators. *Phys Rev B* 2012; **86**: 115112.
36. Hirsch J and Marsiglio F. Hole superconductivity in infinite-layer nickelates. *Physica C Supercond* 2019; **566**: 1353534.
37. Sakakibara H, Usui H and Suzuki K *et al.* Model construction and a possibility of cupratelike pairing in a new d^9 nickelate superconductor (Nd, Sr) NiO_2 . *Phys Rev Lett* 2020; **125**: 077003.
38. Botana AS and Norman MR. Similarities and differences between LaNiO_2 and CaCuO_2 and implications for superconductivity. *Phys Rev X* 2020; **10**: 011024.
39. Wu X, Di Sante D and Schwemmer T *et al.* Robust $d_{x^2-y^2}$ wave superconductivity of infinite-layer nickelates. *Phys Rev B* 2020; **101**: 060504.
40. Nomura Y, Hirayama M and Tadano T *et al.* Formation of a two-dimensional single-component correlated electron system and band engineering in the nickelate superconductor NdNiO_2 . *Phys Rev B* 2019; **100**: 205138.